Dalton Transactions

ROYAL SOCIETY OF CHEMISTRY

PAPER

View Article Online
View Journal

Cite this: DOI: 10.1039/d6dt00591h

Interaction of bi-nuclear gallium(III) complexes with human serum albumin and impact on potency towards osteosarcoma stem cells

Xiao Feng and Kogularamanan Suntharalingam *

Metastasised osteosarcoma has very poor survival rates, in part due to the presence of osteosarcoma stem cells (OSCs), a resistant subpopulation with self-renewal and differentiation capabilities. Recently, we reported the first metal complex (a bi-nuclear gallium(III) complex comprising tridentate Schiff base ligands and 8-hydroxyquinoline moieties) capable of eliciting an immunogenic response against OSCs. Here, we present an in-depth investigation of the interaction between this anti-OSC bi-nuclear gallium(III) complex and related complexes (**4–7**) with human serum albumin (HSA). Given that HSA is the predominant protein in human blood and that most osteosarcoma drugs are administered intravenously, the interaction of complexes **4–7** with HSA is of significant translational relevance. The binding of complexes **4–7** to HSA was examined using spectroscopic titration experiments. The resulting quenching (K_q) and binding (K_a) constants were in the 10^4–10^5 M^{-1} range, indicating strong binding affinity. Molecular docking studies suggest that representative bi-nuclear gallium(III) complexes **4** and **5** interact with amino acid residues within subdomain IIA, primarily through hydrophobic and π–π interactions. Biophysical analyses indicate that, although the bi-nuclear gallium(III) complexes bind tightly to HSA, they do not induce significant structural perturbations. Notably, HSA binding improves the aqueous solubility of complexes **4–7**. Cytotoxicity studies demonstrate that HSA binding enhances the potency of complexes **4–7** towards both bulk osteosarcoma cells (U2OS) and OSC-enriched cells (U2OS-MTX). Moreover, the HSA-bound bi-nuclear gallium(III) complexes (HSA-**4–7**) more effectively inhibit three-dimensional sarcosphere formation and viability compared to clinically used metallodrugs cisplatin and carboplatin, and the established anti-cancer stem cell agent salinomycin.

Received 10th March 2026,
Accepted 10th April 2026

DOI: 10.1039/d6dt00591h

rsc.li/dalton

Introduction

Osteosarcoma is the most commonly diagnosed malignant bone tumour in paediatric and adolescent patients.[1,2] Osteosarcoma typically arises within long bones, where it demonstrates a strong capacity for early dissemination to distant organs.[3] At the time of presentation, approximately one in five patients already exhibit metastatic sites.[4] Despite advances in treatment, survival outcomes for this patient group remain extremely poor, with only 5–30% of patients surviving beyond five years.[5,6] This highlights a critical unmet need for therapies that specifically address metastatic spread. Increasing attention has focused on a rare tumour-initiating cell fraction, referred to as osteosarcoma stem cells (OSCs), which possess self-renewal properties and are thought to play a central role in osteosarcoma progression and metastasis.[7–9] Importantly, widely used frontline chemotherapeutic agents such as methotrexate, cisplatin, and doxorubicin may inadvertently favour the persistence or expansion of OSCs, thereby enhancing metastatic potential rather than eliminating it.[10,11] These observations indicate that therapeutic strategies targeting only the bulk osteosarcoma population are unlikely to achieve durable outcomes. Instead, complete eradication of osteosarcoma requires effective targeting of OSCs alongside differentiated bulk osteosarcoma cells. Although multiple OSC-related pathways and molecular targets have been described, translation of these findings into clinically effective agents with acceptable systemic toxicity has not yet been achieved by either academic research efforts or the pharmaceutical industry.[7–9]

Recently we demonstrated that metal-based compounds can effectively eliminate OSCs *in vitro*.[12–15] In particular, we identified a family of gallium(III) complexes coordinated to polypyridyl ligands that exhibited strong cytotoxic activity against both differentiated bulk osteosarcoma cells and OSCs at nanomolar concentrations.[12] Interest in gallium(III) as a

School of Chemistry, University of Leicester, Leicester, LE1 7RH, UK.
E-mail: k.suntharalingam@leicester.ac.uk

therapeutic scaffold was driven by two key considerations: the inherent propensity of gallium salts to localise within bone tissue, and the favourable tolerability profiles reported for gallium(III) compounds previously evaluated in clinical settings.[16–18] Among the compounds tested, the lead gallium (III) complex (**1**, Fig. 1A) demonstrated exceptional potency, displaying more than a 400-fold increase in activity relative to cisplatin against methotrexate-resistant OSCs, while exhibiting markedly reduced toxicity toward non-malignant cells derived from lung, breast, skin, and kidney tissues.[12] Subsequent mechanistic investigations revealed that this compound exerted its cytotoxic effects by translocating to the nucleus and inducing DNA damage, ultimately triggering apoptotic cell death.[12]

Building on these findings, we next designed a series of gallium(III)-polypyridyl complexes incorporating the non-steroidal anti-inflammatory drugs salicylic acid and diflunisal (**2** and **3**, Fig. 1A), with the objective of enhancing OSC-targeted activity.[13,14] NSAIDs function as inhibitors of cyclooxygenase-2 (COX-2), an enzyme responsible for prostaglandin synthesis and a recognised mediator of inflammatory signalling.[19,20] Importantly, COX-2 levels are significantly upregulated in OSCs relative to bulk osteosarcoma cells and COX-2 is considered critical for the maintenance of stem-like properties within OSCs.[21,22] The diflunisal-containing gallium(III) complex **3** displayed particularly pronounced activity, achieving up to three orders of magnitude greater potency against OSCs in both monolayer and sarcosphere assays compared with drugs currently used in first-line (doxorubicin and cisplatin) and second-line (etoposide, ifosfamide, and carboplatin) osteosarcoma therapy.[13] Mechanistic studies indicated that this enhanced efficacy arose from a dual mode of action involving concurrent COX-2 inhibition and nuclear DNA damage.[13]

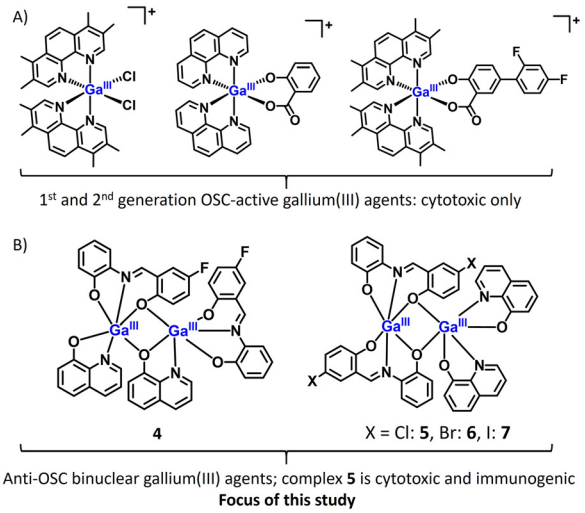

Fig. 1 (A) Chemical structures of mono-nuclear gallium(III)-polypyridyl complexes **1–3** (**2** and **3** with additional nonsteroidal anti-inflammatory drugs motifs) with cytotoxicity towards OSCs. (B) Chemical structures of bi-nuclear gallium(III) complexes **4–7** comprising of tridentate Schiff base ligands and 8-hydroxyquinoline moieties, which are the focus of this study. Complex **5** displays anti-OSC immunotherapeutic properties.

Owing to the natural propensity of gallium salts to localise within bone tissue, we hypothesised that multinuclear gallium (III) architectures could be exploited for targeted activity in bone-associated malignancies. In support of this concept, we very recently reported a series of bi-nuclear gallium(III) complexes bearing tridentate Schiff base ligands in combination with 8-hydroxyquinoline (**4–7**, Fig. 1B). The bi-nuclear gallium (III) complexes demonstrated strong bone affinity and markedly enhanced activity (up to 38-fold) against OSC sarcospheres compared to cisplatin.[15] Notably, the lead compound from this series (**5**, Fig. 1B) exhibited a unique cytotoxic profile, inducing osteosarcoma cell death through a combination of caspase-mediated apoptosis and paraptosis.[15] This dual mechanism triggered the release of danger-associated molecular patterns (DAMPs) characteristic of immunogenic cell death (ICD).[15] In addition, both bulk osteosarcoma cells and OSCs exposed to **5** were readily engulfed by immune cells, providing clear evidence of immune activation.[15] To our knowledge, **5** represents the first example of a metal-based agent capable of eliciting an immunogenic response in both bulk osteosarcoma cells and OSCs. In the context of future translation and taking into consideration that most osteosarcoma chemotherapeutics are administered intravenously,[23] in this study we sought to investigate the interaction of the bi-nuclear gallium(III) complexes **4–7** with human serum albumin (HSA), the most abundant protein in human blood,[24] and its impact on bulk osteosarcoma cell and OSC toxicity. HSA has been widely reported to reversibly bind small molecule anticancer agents (including the investigational gallium(III)-based metallodrug, KP46)[25–28] and accumulate in the tumour microenvironment, potentially enabling selective delivery to cancer cells. Specifically, herein we provide a comprehensive biophysical and computational docking analysis of the interaction of **4–7** and HSA and explore the potency of HSA-bound **4–7** (HSA-**4–7**) towards bulk osteosarcoma cells and OSCs grown in two- and three-dimensional cultures.

Results and discussion

Spectroscopic analysis of the binding of bi-nuclear gallium(III) complexes with human serum albumin

The bi-nuclear gallium(III) complexes **4–7** used in our investigations were synthesised using our previously reported protocols.[15] There are now a number of deposited structures of HSA in the Protein Data Bank (PDB) enabling a thorough understanding of its architecture.[29,30] HSA consists of three structurally similar domains (I, II, III) which each have two subdomains with cavities for binding small molecules. HSA displays distinctive emission (λ_{ex} = 280 nm, λ_{em} = 335 nm) owing largely to the tryptophan residue (Trp214) present in subdomain IIA.[31] The interaction of small molecules with HSA within subdomain IIA can affect HSA emission, depending on the vicinity of binding to the Trp214 residue.

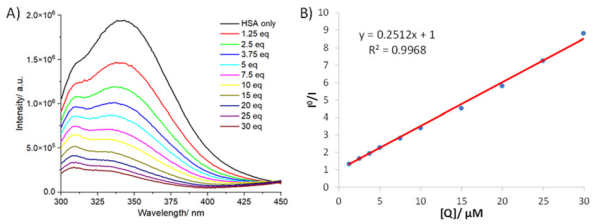

Fig. 2 (A) Representative emission spectra of HSA (1 μM) upon addition of aliquots of **4** (up to 30 μM). (B) *I°/I versus* [*Q*] plot corresponding to the emission data for HSA (1 μM) upon addition of **4**. The gradient was used to calculate the quenching constant (K_q).

We initially explored the binding of the bi-nuclear gallium(III) complexes **4–7** with HSA using fluorescence spectroscopy titration experiments. The fluorescence associated to HSA (λ_{ex} = 280 nm, λ_{em} = 345 nm, 1 μM) decreased upon addition of **4–7** (up to 30 μM) (Fig. 2 and S1–S3). The quenching constant (K_q) and the bimolecular quenching rate constant (k_q) for **4–7** were determined by Stern–Volmer analysis (see SI for equations applied), and are reported in Table 1.[32] The quenching constants K_q for **4–7** varied from 2.51×10^5 to 9.83×10^5 M^{-1}, increasing along with the size of the halogen substituent on **4–7** and their respective log *P* values, **4** (F, log *P* = 1.51 ± 0.001) < **5** (Cl, log *P* = 1.86 ± 0.05) < **6** (Br, log *P* = 1.90 ± 0.002) < **7** (I, log *P* = 2.10 ± 0.03). This suggests that the relative hydrophobicity of **4–7** influences its interaction with HSA. The calculated quenching constants K_q for **4–7** are comparable to those reported for small molecules that bind strongly to subdomain IIA in HSA.[33–36] The bimolecular quenching rate constant k_q for **4–7** varied from 4.93×10^{13} to 1.93×10^{14} M^{-1} s^{-1}, indicative of static quenching (typically assigned when $k_q > 2 \times 10^{10}$ M^{-1} s^{-1}).[37] Complementary UV-vis spectroscopic analysis showed that there were significant changes in the UV-vis trace of HSA in the presence of **4–7** (Fig. S4), suggestive of static quenching. Dynamic quenching is typically associated to no changes to the absorption spectra of fluorophores. The binding constant (K_a) for **4–7** to HSA and the number of binding sites (*n*) were determined using the modified Stern–Volmer analysis (Fig. S5, see SI for equations applied) and are summarised in Table 1.[38] The binding constants (K_a) of **4–7** to HSA were in the 10^4 to 10^5 M^{-1} range comparable to other coordination complexes and suggestive of strong binding.[33,35,39–41] The number of binding sites (*n*) for **4–6** was close to 1 indicating that **4–6** bind to a single site in HSA. The number of binding sites (*n*) for **7** was close to 0.75 suggestive of a 4 : 3 binding ratio between **7** and HSA. Job plot analysis further confirmed that **4–6** bind to HSA in 1 : 1 manner and that **7** binds to HSA with a slightly lower binding ratio (Fig. S6).

Table 1 Quenching constants (K_q), bimolecular quenching rate constants (k_q), binding constants (K_a), and the number of binding sites (*n*) for the interaction of **4–7** with HSA

Agent	K_q/M^{-1}	k_q/M^{-1} s^{-1}	$K_a \times 10^5/M^{-1}$	*n*
HSA-**4**	2.51×10^5	4.93×10^{13}	2.08×10^5	0.98
HSA-**5**	6.74×10^5	1.32×10^{14}	3.16×10^5	0.93
HSA-**6**	7.43×10^5	1.46×10^{14}	1.92×10^5	0.87
HSA-**7**	9.83×10^5	1.93×10^{14}	4.18×10^4	0.72

To gain structural insight into the binding of **4–7** to HSA, synchronous fluorescence studies were conducted. The difference between the excitation and emission wavelengths ($\Delta\lambda = \lambda_{em} - \lambda_{ex}$) indicates the type of chromophores involved in the interaction. When $\Delta\lambda$ = 15 nm, tyrosine residues are involved and when $\Delta\lambda$ = 60 nm, tryptophan residues are involved.[42] The fluorescence intensity of HSA, when $\Delta\lambda$ = 15 nm, decreased between 21.8–81.1% with no shift upon addition of **4–7** (up to 5 μM) (Fig. S7–S10 and Table S1). This is reflective of little transformation around the tyrosine residues. When $\Delta\lambda$ = 60 nm, the fluorescence intensity of HSA decreased between 57.3–94.1% with a modest red-shift (2–3 nm) upon addition of **4–7** (up to 5 μM) (Fig. S7–S10 and Table S1). This is implicative of a structural change that shifts the tryptophan residues to a more polar environment. The difference in the synchronous fluorescence studies when $\Delta\lambda$ = 15 nm and $\Delta\lambda$ = 60 nm suggests that **4–7** binds to HSA preferably in a hydrophobic cavity in close proximity to the tryptophan residue (Trp214) present in the subdomain IIA.

Molecular docking analysis of the binding of bi-nuclear gallium(III) complexes with human serum albumin

Molecular docking studies were conducted to gain deeper, molecular-level insight into the non-covalent interactions between the bi-nuclear gallium(III) complexes and HSA. Given that the ligands surrounding the gallium(III) centres in **4** and **5–7** adopt different arrangements (Fig. 1B), molecular docking analyses were performed using the previously reported X-ray crystal structure of **4** and **5**, with **5** serving as a representative of the other structurally similar bi-nuclear gallium(III) complexes in the series. The HSA protein scaffold derived from the crystal structure with PDB entry 1H9Z[43] was used to perform a broad, unbiased search for potential binding interactions of **4** and **5**. The optimal binding conformations of **4** and **5** in complex with HSA are shown in Fig. 3. The lowest total free binding energy obtained for the conformations of **4** and **5** in complex with HSA are −8.40 kcal mol^{-1} and −9.21 kcal mol^{-1}, respectively. Both **4** and **5** were found to bind to HSA within subdomain IIA (also known as Sudlow site I), a well-established small molecule binding site (Fig. 3A and C). The bi-nuclear gallium(III) complexes **4** and **5** interact with amino acid residues in subdomain IIA through hydrophobic and π–π interactions (Fig. 3B and D). Specifically, one of the 8-hydroxyquinoline units and one of the fluorophenyl moieties in **4** engages with Leu203 and Ala201, respectively *via* hydrophobic interactions. Additionally, one of the unsubstituted phenyl moieties in **4** interacts with Tyr148 through π–π interactions (dihedral angle, *Φ* of 45.3° between the least-squares planes and a centroid–centroid distance, *d* of 4.6 Å). For **5**, both of the chlorophenyl moieties in **5** interact with Leu203 and Ala201 *via* hydrophobic interactions. Furthermore, one of the

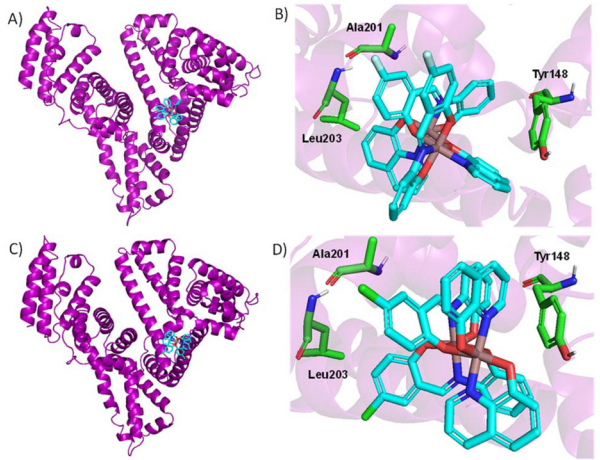

Fig. 3 Docking studies of **4** and **5** with HSA using Autodock 4.0. (A) Lowest energy structure for **4** bound to HSA. (B) Image of **4** interacting with amino acids within subdomain IIA (Sudlow site I) *via* hydrophobic and π–π interactions. (C) Lowest energy structure for **5** bound to HSA. (D) Image of **5** interacting with amino acids within subdomain IIA (Sudlow site I) *via* hydrophobic and π–π interactions.

unsubstituted phenyl moieties in **5** interacts with Tyr148 through π–π interactions (dihedral angle, Φ of 43.8° between the least-squares planes and a centroid–centroid distance, d of 4.8 Å). The two gallium(III) centres in **4** and **5** are located approximately 1.6–2.0 nm away from Trp214 (Fig. S11), enabling quenching of tryptophan fluorescence, consistent with the emission studies.

Conformational and physical implications on human serum albumin upon binding to bi-nuclear gallium(III) complexes

To understand the overall structural and conformational changes in HSA upon binding to the bi-nuclear gallium(III) complexes, further biophysical studies were conducted. To decipher if **4–7** binding leads to HSA unfolding or cleavage, SDS-PAGE electrophoresis studies were carried out. Upon incubation of HSA (5 μM) with **4–7** (5 μM) at 37 °C for 24 h, there was no indication of HSA unfolding or cleavage (Fig. S12). This suggests that although **4–7** binds tightly to HSA leading to structural modifications around the tryptophan residues (as indicated in the synchronous fluorescence studies), this does not result in unfolding or cleavage. Dynamic light scattering (DLS) studies were also performed with HSA (100 μM) in the absence and presence of **5** (100 μM), taken as a representative member of the bi-nuclear gallium(III) complex series, upon incubation at 37 °C for 24 h. The DLS size distribution profile for HSA (100 μM) in PBS (pH 7.4) exhibited peaks corresponding to the monomeric, dimeric, and aggregate forms, with an average diameter of 8.077 nm (PDI = 0.449) (Fig. S13A), consistent with previous reports.[44] In the presence of **5**, the DLS size distribution profile remained largely unchanged, showing only a slight increase in the average diameter to 8.514 nm (PDI = 0.469) (Fig. S13B). This indicates that binding of **5** to HSA does not induce significant structural or conformational rearrangements, in agreement with the SDS-PAGE electrophoresis results. Complementary transmission electron microscopy (TEM) studies were performed to evaluate the effect of **5** binding to HSA on its surface morphology and globule size distribution. The TEM image of HSA (100 μM) alone revealed aggregation, which remained largely unperturbed in the presence of **5** (100 μM) (Fig. S14), further supporting that binding of **5** to HSA does not induce major structural modifications.

Taken together, the SDS-PAGE electrophoresis, DLS, and TEM studies suggest that although the bi-nuclear gallium(III) complexes bind to HSA, they do not induce dramatical structural modifications. This bodes well for the possible transport of the bi-nuclear gallium(III) complexes into bulk osteosarcoma cells and OSCs by HSA. One of the ways by which HSA is known to enhance the delivery of small-molecule therapeutics is by improving their aqueous solubility. Therefore, the impact of HSA binding on the solubility of **4–7** was evaluated. In water : DMSO solution (200 : 1), the saturation concentration of **4–6** was 100 μM, while that of **7** was 50 μM. However, upon pre-incubation with HSA (1 : 1 molar ratio, 30 min) to form HSA-loaded **4–7**, concentrations of up to 500 μM could be readily achieved (Fig. S15–S18). This shows that upon binding to HSA, the aqueous solubility of **4–7** is significantly improved.

Cytotoxicity towards monolayer cultured bulk osteosarcoma cells and osteosarcoma stem cells

The impact of HSA binding on the potency of the bi-nuclear gallium(III) complexes **4–7** towards monolayer cultured bulk osteosarcoma cells and OSCs was determined using the MTT [3-(4,5-dimethylthiazol-2-yl)-2,5-diphenyltetrazolium bromide] assay. To conduct the cytotoxicity studies the bi-nuclear gallium(III) complexes **4–7** were pre-incubated with HSA (1 : 1 molar ratio, 30 min) prior to administration to bulk osteosarcoma cells (U2OS) and OSC-enriched cells (U2OS-MTX). The IC_{50} values (half-maximal inhibitory concentration) were derived from dose–response curves (Fig. S19 and S20) and are summarised in Table 2. The HSA-bound bi-nuclear gallium(III) complexes (HSA-**4**, HSA-**5**, HSA-**6**, and HSA-**7**) displayed micromolar IC_{50} values towards U2OS and

Table 2 IC_{50} values of HSA-bound bi-nuclear gallium(III) complexes HSA-**4–7**, cisplatin, carboplatin, and salinomycin against U2OS and U2OS-MTX cells and U2OS-MTX sarcospheres determined after 3 or 10 days incubation (mean of three independent experiments ± SD)

Agent	U2OS IC_{50} [μM]	U2OS-MTX IC_{50} [μM]	OSC-sarcosphere IC_{50} [μM]
HSA-**4**	2.50 ± 0.11	3.10 ± 0.08	0.99 ± 0.14
HSA-**5**	2.37 ± 0.11	2.97 ± 0.47	0.66 ± 0.01
HSA-**6**	3.90 ± 0.16	3.54 ± 0.36	1.72 ± 0.09
HSA-**7**	2.79 ± 0.23	4.12 ± 0.46	2.24 ± 0.05
Cisplatin[a]	16.30 ± 0.50	33.87 ± 3.71	16.49 ± 0.20
Carboplatin[a]	157.50 ± 2.21	114.98 ± 2.31	22.77 ± 0.09
Salinomycin[a]	6.09 ± 1.06	1.49 ± 0.26	4.70 ± 0.08

[a] Taken from ref. 12.

U2OS-MTX cells. The HSA-bound bi-nuclear gallium(III) complexes HSA-**4**–**7** all exhibited greater potency towards U2OS and U2OS-MTX cells than unbound **4**–**7** (Table 2 and Table S2),[15] suggesting that the binding of **4**–**7** to HSA enhances toxicity towards bulk osteosarcoma cells and OSCs. Notably the HSA-bound bi-nuclear gallium(III) complexes HSA-**4**–**7** were largely equipotent towards U2OS and U2OS-MTX cells whereas unbound **4**–**7** were slightly more potent toward U2OS cells than U2OS-MTX cells (Table 2 and Table S2). This shows that the binding of **4**–**7** to HSA not only improves potency towards OSCs but also improves selectivity over bulk osteosarcoma cells (Table 2 and Table S2). Within the HSA-bound bi-nuclear gallium(III) complexes, HSA-**5** displayed the lowest IC_{50} values toward U2OS and U2OS-MTX cells (Table 2). HSA-**5** was 6.9-fold and 66.5-fold more potent than cisplatin and carboplatin towards U2OS cells ($p < 0.05$, $n = 18$) and 11.4-fold and 38.7-fold more potent than cisplatin and carboplatin towards U2OS-MTX cells ($p < 0.05$, $n = 18$) (Table 2).[12] Although HSA-**5** displayed 2.6-fold higher potency towards U2OS cells than the gold standard anti-cancer stem cell agent salinomycin ($p < 0.05$, $n = 18$), HSA-**5** was 2.0-fold less potent towards U2OS-MTX cells than salinomycin (Table 2). Control studies showed that HSA alone was non-toxic towards U2OS and U2OS-MTX cells within the concentration range tested (IC_{50} > 100 μM) (Fig. S21), proving that the cytotoxicity observed for HSA-**4**–**7** is due to the bound bi-nuclear gallium(III) complexes **4**–**7**.

Activity toward three-dimensionally cultured sarcospheres

In light of the promising potency of the HSA-bound bi-nuclear gallium(III) complexes HSA-**4**–**7** towards OSC-enriched cells cultured as monolayers, their activity was further assessed in 3D-cultured OSC-enriched sarcospheres. Under low-attachment, serum-free conditions, U2OS-MTX cells form sarcospheres, irregular aggregates of OSCs that serve as physiologically relevant *in vitro* mimics of osteosarcomas *in vivo*.[11] Treatment of single cell suspensions of U2OS-MTX cells with the HSA-bound bi-nuclear gallium(III) complexes HSA-**4**–**7** (at their corresponding IC_{20} value for 10 days) noticeably decreased the formation of sarcospheres compared to untreated control cells (Fig. 4). Under identical conditions cisplatin (IC_{20} value, 10 days) displayed limited sarcosphere inhibition whereas salinomycin (IC_{20} value, 10 days) impaired sarcosphere formation to a similar extent as HSA-**4**–**7** (Fig. 4 and S22). The effect of HSA-**4**–**7** on sarcosphere viability was evaluated using the resazurin-based colorimetric reagent TOX8. Analysis of dose–response curves revealed that HSA-**4**–**7** possessed low-micromolar to sub-micromolar potency against sarcospheres (Table 2 and Fig. S23). Based on the IC_{50} values, HSA-**4**–**7** were appreciably more potent toward three-dimensionally cultured sarcospheres than U2OS-MTX cells grown in monolayer cultures. This suggests that binding of **4**–**7** to HSA enables efficient penetration of the multicellular sarcosphere architecture. Notably, the most potent HSA-bound bi-nuclear gallium(III) complex, HSA-**5** displayed significantly higher potency toward sarcospheres than cisplatin (25.0-fold, $p < 0.05$), carboplatin (34.5-fold, $p < 0.05$), and salinomycin (7.1-fold, $p < 0.05$).[12]

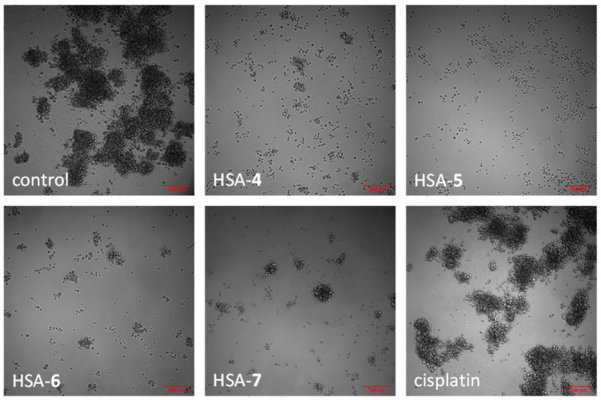

Fig. 4 Representative bright-field images (10×) of U2OS-MTX sarcospheres in the absence and presence of HSA-**4**–**7** and cisplatin at its IC_{20} value (10 days incubation) scale bar = 100 μm.

Conclusions

Overall, our spectroscopic, molecular docking, and biophysical analyses of bi-nuclear gallium(III) complexes **4**–**7** binding to HSA indicate that these complexes bind tightly within subdomain IIA, predominantly through hydrophobic and π–π interactions. Although the bi-nuclear gallium(III) complexes **4**–**7** display relatively large quenching constants (K_q, 10^5 M^{-1} range), binding constants (K_a, 10^4–10^5 M^{-1} range), and bimolecular quenching rate constants (k_q, 10^{13}–10^{14} M^{-1} s^{-1} range), their binding does not induce major structural modifications in HSA. This supported the potential role of HSA in transporting **4**–**7** into bulk osteosarcoma cells and OSCs. The HSA-bound bi-nuclear gallium(III) complexes HSA-**4**–**7** displayed significantly better aqueous solubility than unbound **4**–**7**, indicating that HSA binding enhances the bioavailability of **4**–**7**. HSA binding also enhances the potency of the bi-nuclear gallium (III) complexes against bulk osteosarcoma cells and OSCs compared to their unbound counterparts. Within the HSA-bound bi-nuclear gallium(III) complexes, HSA-**5** exhibited the greatest potency, up to 66.5-fold and 38.7-fold more potent than cisplatin and carboplatin towards bulk osteosarcoma cells and OSCs respectively. Under three-dimensional culture conditions, HSA-**4**–**7** markedly decreased sarcosphere viability at low micromolar and sub-micromolar concentrations. HSA-**4**–**7** were up to 4.5-fold more potent against sarcospheres than monolayer-cultured OSCs, highlighting their ability to penetrate complex multicellular osteosarcoma assemblies. Strikingly, HSA-**4**–**7** exhibited up to 34.5-fold greater activity towards sarcospheres than cisplatin, carboplatin, and salinomycin. Taken together, our results demonstrate that bi-nuclear gallium(III) complexes **4**–**7** bind strongly to HSA, and that this interaction positively impacts their potency toward OSCs cultured in both monolayer and three-dimensional systems.

Author contributions

Conceptualisation, K. S.; methodology, K. S. and X. F.; validation, K. S. and X. F.; formal analysis, K. S. and X. F.; investigation, K. S. and X. F.; writing – original draft preparation, K. S. and X. F.; writing – review and editing, K. S. and X. F.; supervision, K. S.; project administration, K. S.; funding acquisition, K. S. All authors have read and agreed to the published version of the manuscript.

Conflicts of interest

There are no conflicts to declare.

Data availability

The data supporting this article have been included as part of the supplementary information (SI). Supplementary information is available. See DOI: https://doi.org/10.1039/d6dt00591h.

Acknowledgements

K. S. is supported by EPSRC New Investigator Award (EP/S005544/1). X. F. is supported by a Chinese Scholarship Council PhD studentship. The Advanced Imaging Facility (RRID:SCR_020967) at the University of Leicester is also thanked.

References

1 A. K. Raymond, *Pathology and genetics Tumours of Soft Tissue and Bone*, World Health Organization classification of tumours, 2002, pp. 264–270.
2 V. Y. Jo and C. D. M. Fletcher, *Pathology*, 2014, **46**, 95–104.
3 G. Sheng, Y. Gao, Y. Yang and H. Wu, *Front. Oncol.*, 2021, **11**, 780264.
4 G. Bacci, M. Rocca, M. Salone, A. Balladelli, S. Ferrari, E. Palmerini, C. Forni and A. Briccoli, *J. Surg. Oncol.*, 2008, **98**, 415–420.
5 L. Mirabello, R. J. Troisi and S. A. Savage, *Int. J. Cancer*, 2009, **125**, 229–234.
6 American Cancer Society, Survival Rates for Osteosarcoma, (accessed Feburary 2026) https://www.cancer.org/cancer/bone-cancer/detection-diagnosis-staging/survival-statistics.
7 G.-N. Yan, Y.-F. Lv and Q.-N. Guo, *Cancer Lett.*, 2016, **370**, 268–274.
8 H. K. Brown, M. Tellez-Gabriel and D. Heymann, *Cancer Lett.*, 2017, **386**, 189–195.
9 V. A. Siclari and L. Qin, *J. Orthop. Surg. Res.*, 2010, **5**, 78.
10 S. R. Martins-Neves, D. I. Paiva-Oliveira, P. M. Wijers-Koster, A. J. Abrunhosa, C. Fontes-Ribeiro, J. V. Bovee, A. M. Cleton-Jansen and C. M. Gomes, *Cancer Lett.*, 2016, **370**, 286–295.
11 Q. L. Tang, Y. Liang, X. B. Xie, J. Q. Yin, C. Y. Zou, Z. Q. Zhao, J. N. Shen and J. Wang, *Chin. J. Cancer*, 2011, **30**, 426–432.
12 P. Robin, K. Singh and K. Suntharalingam, *Chem. Commun.*, 2020, **56**, 1509–1512.
13 Z. Xiao, G. Passeri, J. Northcote-Smith, K. Singh and K. Suntharalingam, *Chem. – Eur. J.*, 2021, **27**, 13846–13854.
14 R. A. Vincent, G. Passeri, J. Northcote-Smith, K. Singh and K. Suntharalingam, *ChemBioChem*, 2022, **23**, e202200532.
15 X. Feng, S. Dhandore, Y. Liu, K. Singh, F. Ortu and K. Suntharalingam, *Chem. – Eur. J.*, 2025, **31**, e202500747.
16 C. R. Chitambar, *Expert Opin. Invest. Drugs*, 2004, **13**, 531–541.
17 C. R. Chitambar, *Future Med. Chem.*, 2012, **4**, 1257–1272.
18 C. R. Chitambar, *Met. Ions Life Sci.*, 2018, **18**, 281–301.
19 S. B. Abramson and G. Weissmann, *Arthritis Rheum.*, 1989, **32**, 1–9.
20 C. A. Rouzer and L. J. Marnett, *J. Lipid Res.*, 2009, **50**(Suppl), S29–S34.
21 H. Urakawa, Y. Nishida, T. Naruse, H. Nakashima and N. Ishiguro, *Clin. Orthop. Relat. Res.*, 2009, **467**, 2932–2938.
22 L. Y. Pang, E. L. Gatenby, A. Kamida, B. A. Whitelaw, T. R. Hupp and D. J. Argyle, *PLoS One*, 2014, **9**, e83144.
23 D. Carrle and S. S. Bielack, *Int. Orthop.*, 2006, **30**, 445–451.
24 R. N. Moman, N. Gupta and M. A. Varacallo, in *StatPearls*, Treasure Island (FL), 2025.
25 F. Kratz and U. Beyer, *Drug Delivery*, 1998, **5**, 281–299.
26 G. Sudlow, D. J. Birkett and D. N. Wade, *Mol. Pharmacol.*, 1975, **11**, 824–832.
27 É. A. Enyedy, O. Dömötör, K. Bali, A. Hetényi, T. Tuccinardi and B. K. Keppler, *J. Biol. Inorg. Chem.*, 2015, **20**, 77–88.
28 A. A. Hummer, C. Bartel, V. B. Arion, M. A. Jakupec, W. Meyer-Klaucke, T. Geraki, P. D. Quinn, A. Mijovilovich, B. K. Keppler and A. Rompel, *J. Med. Chem.*, 2012, **55**, 5601–5613.
29 S. Curry, *Drug Metab. Pharmacokinet.*, 2009, **24**, 342–357.
30 M. Fasano, S. Curry, E. Terreno, M. Galliano, G. Fanali, P. Narciso, S. Notari and P. Ascenzi, *IUBMB Life*, 2005, **57**, 787–796.
31 K. Jankeje, M. Amiri and J. R. Albani, Relation between Human Serum Albumin Structure and Fluorescence Decay Parameters of Tryptophan Residue 214, in *Encyclopedia of Analytical Chemistry*, 2017.
32 J. R. Lakowicz, *Principles of Fluorescence Spectroscopy*, Springer, 2006.
33 S. U. Parsekar, K. Paliwal, P. Haldar, P. K. S. Antharjanam and M. Kumar, *ACS Omega*, 2022, **7**, 2881–2896.
34 J. Kang, Y. Liu, M. X. Xie, S. Li, M. Jiang and Y. D. Wang, *Biochim. Biophys. Acta*, 2004, **1674**, 205–214.
35 A. Hussain, M. F. AlAjmi, M. T. Rehman, S. Amir, F. M. Husain, A. Alsalme, M. A. Siddiqui, A. A. AlKhedhairy and R. A. Khan, *Sci. Rep.*, 2019, **9**, 5237.
36 J. Tian, J. Liu, J. Xie, X. Yao, Z. Hu and X. Chen, *J. Photochem. Photobiol., B*, 2004, **74**, 39–45.

37 M. S. Ali and H. A. Al-Lohedan, *J. Mol. Liq.*, 2014, **197**, 124–130.
38 S. S. Lehrer, *Biochemistry*, 1971, **10**, 3254–3263.
39 A.-C. Munteanu, M. Badea, R. Olar, L. Silvestro, M. Mihaila, L. I. Brasoveanu, M. G. Musat, A. Andries and V. Uivarosi, *Appl. Organomet. Chem.*, 2018, **32**, e4579.
40 N. Shahabadi, S. M. Fili and S. Kashanian, *J. Coord. Chem.*, 2018, **71**, 329–341.
41 T. Topala, A. Bodoki, L. Oprean and R. Oprean, *Clujul Med.*, 2014, **87**, 215–219.
42 J. Miller, *Proc. Anal. Div. Chem. Soc.*, 1979, **16**, 203–208.
43 I. Petitpas, A. A. Bhattacharya, S. Twine, M. East and S. Curry, *J. Biol. Chem.*, 2001, **276**, 22804–22809.
44 A. I. Luik, Y. N. Naboka, S. E. Mogilevich, T. O. Hushcha and N. I. Mischenko, *Spectrochim. Acta, Part A*, 1998, **54A**, 1503–1507.